Cell

Resource

Genome-Wide High-Resolution Mapping of Exosome Substrates Reveals Hidden Features in the *Arabidopsis* Transcriptome

Julia A. Chekanova,[1,2,8,13] Brian D. Gregory,[3,4,8] Sergei V. Reverdatto,[2] Huaming Chen,[4] Ravi Kumar,[1] Tanya Hooker,[1] Junshi Yazaki,[3,4] Pinghua Li,[2,10] Nikolai Skiba,[5,9] Qian Peng,[3,6] Jose Alonso,[3,11] Vladimir Brukhin,[7,12] Ueli Grossniklaus,[7] Joseph R. Ecker,[3,4,*] and Dmitry A. Belostotsky[1,2,13,*]

[1]School of Biological Sciences, University of Missouri—Kansas City, Kansas City, MO 64110, USA
[2]Department of Biological Sciences, State University of New York at Albany, Albany, NY 12222, USA
[3]Plant Biology Laboratory
[4]Genomic Analysis Laboratory
The Salk Institute for Biological Studies, La Jolla, CA 92037, USA
[5]Howe Laboratory of Ophthalmology, Harvard Medical School, Boston, MA 02114, USA
[6]Department of Computer Science and Engineering, University of California San Diego, La Jolla, CA 92037, USA
[7]Institute of Plant Biology and Zürich-Basel Plant Science Centre, University of Zurich, CH-8008 Zurich, Switzerland
[8]These authors contributed equally to this work.
[9]Present address: Albert Eye Research Institute, Duke University Eye Center, Durham, NC 27710, USA.
[10]Present address: Department of Molecular Biology, Cornell University, Ithaca, NY 14853.
[11]Present address: Department of Genetics, North Carolina State University, Raleigh, NC 27695, USA.
[12]Present address: Department of Plant Biology, University of Illinois, Urbana, IL 61801, USA.
[13]Present address: School of Biological Sciences, University of Missouri—Kansas City, Kansas City, MO 64110, USA.
*Correspondence: ecker@salk.edu (J.R.E.), belostotskyd@umkc.edu (D.A.B.)
DOI 10.1016/j.cell.2007.10.056

SUMMARY

The exosome complex plays a central and essential role in RNA metabolism. However, comprehensive studies of exosome substrates and functional analyses of its subunits are lacking. Here, we demonstrate that as opposed to yeast and metazoans the plant exosome core possesses an unanticipated functional plasticity and present a genome-wide atlas of *Arabidopsis* exosome targets. Additionally, our study provides evidence for widespread polyadenylation- and exosome-mediated RNA quality control in plants, reveals unexpected aspects of stable structural RNA metabolism, and uncovers numerous novel exosome substrates. These include a select subset of mRNAs, miRNA processing intermediates, and hundreds of noncoding RNAs, the vast majority of which have not been previously described and belong to a layer of the transcriptome that can only be visualized upon inhibition of exosome activity. These first genome-wide maps of exosome substrates will aid in illuminating new fundamental components and regulatory mechanisms of eukaryotic transcriptomes.

INTRODUCTION

The exosome is an evolutionarily conserved macromolecular complex that mediates numerous reactions of 3′–5′ RNA processing and degradation and is essential for viability (Estevez et al., 2003; Mitchell et al., 1997). Loss of any individual subunit of its nine-component core is lethal in *S. cerevisiae* and causes near-identical profiles of RNA-processing defects (Allmang et al., 1999a, 1999b). Moreover, X-ray crystallographic analysis of the human exosome indicates that all nine core subunits are required for its integrity (Liu et al., 2006).

The salient feature of the exosome core is the hexameric ring defined by heterodimers of the RNase PH domain-type proteins RRP41-RRP45, MTR3-RRP42, and RRP43-RRP46. These heterodimers are bridged on one side by three subunits containing S1 and KH domains: RRP40 links RRP45 and RRP46, RRP4 interacts with RRP41 and RRP42, and CSL4 contacts MTR3 and RRP43. Surprisingly, all six RNase PH-type proteins in yeast and human complexes are catalytically inactive and serve to mediate interactions with RRP44 (Dis3), a 3′–5′ hydrolytic RNase responsible for most if not all of the catalytic activity of the yeast exosome (Dziembowski et al., 2007; Liu et al., 2007). In contrast, the RRP41 exosome subunit in the plant lineage retained its catalytic competence (Chekanova et al., 2000). Furthermore, RRP44 is stably associated with the core complex in yeast and *Drosophila* but not in human and *T. brucei* (Chen et al., 2001; Estevez et al., 2001, 2003). These

observations hint at a yet to be explored diversity of structure-function relationships in the exosome complex.

Many auxiliary factors interact with the exosome and facilitate its functions. Most of its cytoplasmic activities, such as homeostatic mRNA turnover, decay of unstable mRNAs, nonsense-mediated mRNA decay, as well as the degradation of the mRNA fragments derived from endonucleolytic cleavage by RISC or from no-go decay, are mediated by the SKI2/SKI3/SKI8 complex and the SKI7 protein (reviewed in Houseley et al., 2006). The exosome also has numerous targets in the nucleus. The nuclear exosome is remarkably versatile and is able to carry out precise 3′ end processing of the 5.8S rRNA precursor (Allmang et al., 1999a) but also completely degrades the external transcribed rRNA spacer (Allmang et al., 2000), aberrant pre-rRNAs, pre-mRNAs, and pre-tRNAs (Bousquet-Antonelli et al., 2000; Kadaba et al., 2004, 2006; Libri et al., 2002; Torchet et al., 2002), as well as the normal mRNAs trapped in the nucleus (Das et al., 2003). These processing and degradation activities require distinct auxiliary factors: the putative RNA-binding protein LRP1 participates in the processing of stable RNAs (Mitchell et al., 2003; Peng et al., 2003), while the RNase D-like protein RRP6 is required for all activities of the nuclear exosome. In addition, nuclear RNA degradation is facilitated by the TRAMP (*TR*F4/5-*A*IR1/2-*M*TR4 *p*olyadenylation) complex, which helps recruit the exosome to the various aberrant RNAs (LaCava et al., 2005; Vanacova et al., 2005; Wyers et al., 2005).

Although the exosome is positioned at the nexus of cellular RNA transactions, the extent of conservation of structure-function relationships and the roles of its individual subunits across the phylogenetic spectrum remain unknown. Additionally, elucidation of the mechanistic basis of exosome essentiality is hampered by its functional versatility. Furthermore, exosome substrates have yet to be comprehensively identified in any system, as even the most extensive datasets available only address its nuclear-specific functions and/or are based on microarray platforms that are not genome wide and/or not strand specific (Davis and Ares, 2006; Houalla et al., 2006; Wyers et al., 2005). Here, we present evidence for a unique subfunctionalization of the individual subunits of the plant exosome core and widespread oligoadenylation- and exosome-mediated RNA quality-control pathways in plants. Further, we report the first high-resolution genome-wide map of exosome targets. These targets include multiple classes of stable structural RNAs, a select subset of mRNAs, primary microRNA (pri-miRNA) processing intermediates, tandem repeat-associated siRNA precursor species, as well as numerous noncoding RNAs, many of which can only be revealed through repressing the exosome.

RESULTS AND DISCUSSION

Composition of the *Arabidopsis* Core Exosome

Previously, we demonstrated that *Arabidopsis thaliana* RRP4 and RRP41 proteins physically interact and reside in a high-molecular-weight complex in planta (Chekanova et al., 2000, 2002). To elucidate its composition, we generated transgenic plants expressing either TAP-tagged RRP4 or RRP41 at physiological levels in *rrp4-1* or *rrp41-1* mutant plants, respectively. TAP-tagged RRP4 and RRP41 fully rescued the lethal phenotypes of their corresponding null alleles. TAP-tagged complexes were purified, and polypeptides shared between RRP4-TAP and RRP41-TAP samples but absent from the wild-type (WT) sample were subjected to MALDI and MS/MS analyses. Nine polypeptides corresponding to known subunits of the exosome core were identified: S1 and/or KH domain-containing subunits RRP4, RRP40A, and CSL4 as well as the RNase PH-type subunits RRP41, RRP42, RRP43, RRP45B, RRP46, and MTR3 (Figure 1 and Table S1 available online).

In the case of subunits encoded by duplicated genes, only RRP40A and RRP45B were identified. This may be due to differences in the expression patterns and/or levels between the members of these gene pairs (Hooker et al., 2007). RRP6, which is restricted to a nuclear form of the exosome (Allmang et al., 1999b; Brouwer et al., 2001; Graham et al., 2006) and is likely underrepresented in our preparations, was also absent. On the other hand, the absence of RRP44, which is responsible for most if not all of the catalytic activity of the core exosome in yeast and humans, may reflect a genuine species-specific difference in the functional architecture of the exosome since the *Arabidopsis* RRP41 subunit is unique in retaining its full catalytic activity (Chekanova et al., 2000).

Mutations in the Core Subunits of *Arabidopsis* Exosome Cause Unique Phenotypes

To determine the consequences of losing specific exosome components on plant development, we characterized transfer-DNA (T-DNA) insertional alleles in several core subunits of the *Arabidopsis* exosome. In yeast, the CSL4 subunit is essential for viability (Allmang et al., 1999b; Baker et al., 1998), and X-ray crystallographic analysis of the human exosome predicts that all of its core subunits are critical to maintaining structural integrity and functionality of the complex (Liu et al., 2006). In marked contrast, we found that neither integrity nor function of the *Arabidopsis* exosome was significantly compromised by loss of CSL4. First, neither *csl4-1* nor *csl4-2* (a confirmed null allele) mutant plants manifested any discernible phenotype (Figure S1). Second, size fractionation demonstrated that the *Arabidopsis* exosome complex lacking CSL4 remained nearly intact (Figure 1C). Furthermore, tiling microarray analyses (below) revealed that loss of CSL4 affects only a subset of exosome targets (Figure S2 and Tables S2 and S3). In contrast, *Arabidopsis* RRP41 was essential for development of the female gametophyte, an eight-celled haploid structure derived from the primary product of female meiosis. While the *rrp41-1* mutant allele was normally transmitted through the male parent, it was not transmitted through the female (n = 194), and selfed *rrp41/RRP41* heterozygotes produced

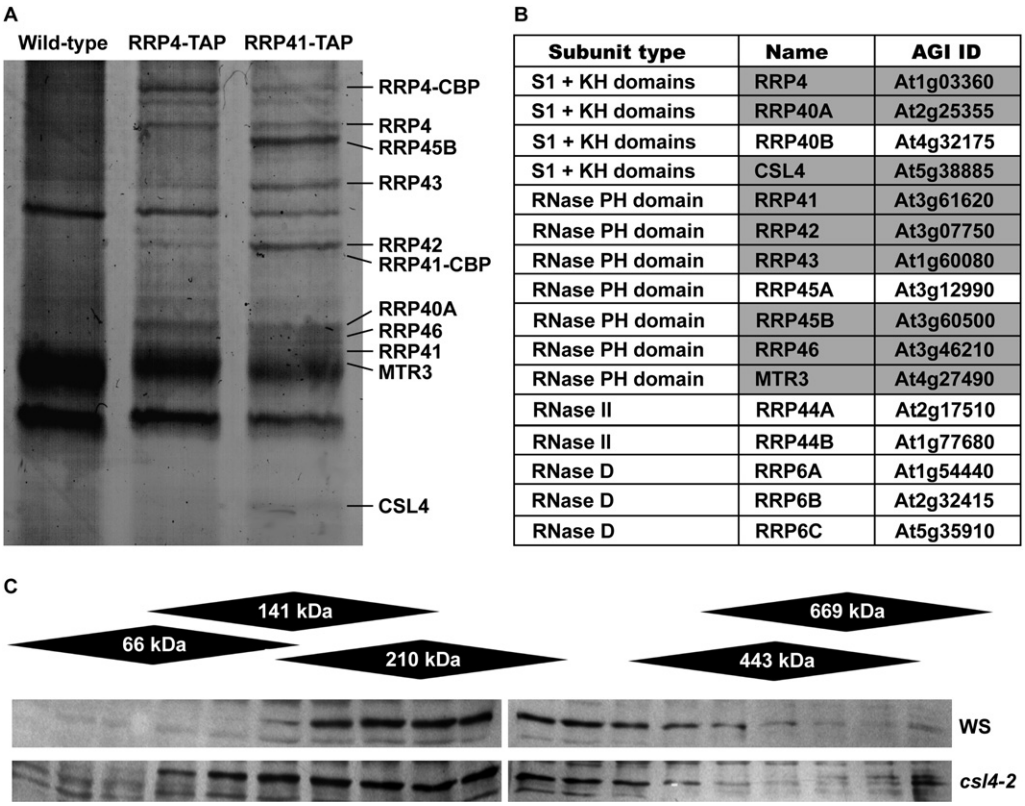

Subunit type	Name	AGI ID
S1 + KH domains	RRP4	At1g03360
S1 + KH domains	RRP40A	At2g25355
S1 + KH domains	RRP40B	At4g32175
S1 + KH domains	CSL4	At5g38885
RNase PH domain	RRP41	At3g61620
RNase PH domain	RRP42	At3g07750
RNase PH domain	RRP43	At1g60080
RNase PH domain	RRP45A	At3g12990
RNase PH domain	RRP45B	At3g60500
RNase PH domain	RRP46	At3g46210
RNase PH domain	MTR3	At4g27490
RNase II	RRP44A	At2g17510
RNase II	RRP44B	At1g77680
RNase D	RRP6A	At1g54440
RNase D	RRP6B	At2g32415
RNase D	RRP6C	At5g35910

Figure 1. Compositional Analysis of *Arabidopsis* Exosome

(A) TAP-tagged preparations from RRP4-TAP, RRP41-TAP, and WT lines. Exosome subunits identified by MS/MS are indicated. Major bands shared between the WT, RRP4-TAP, and RRP41-TAP samples correspond to TEV protease and a common contaminant.

(B) Exosome subunit homologs encoded in the *Arabidopsis* genome; subunits identified in TAP-tagged preparations are shaded.

(C) *Arabidopsis* RRP41 protein (27 kDa) cosediments with a complex of >210 kDa in both Ws and *csl4-2* extracts (calculated molecular weight [MW] of *Arabidopsis* exosome, based on the results of MS/MS, is 274 kDa).

seeds and aborted ovules in a 1:1 ratio (Figures 2A and S3; three independent *rrp41* alleles showed identical phenotypes). Furthermore, the resulting progeny segregated 1:1 for WT and heterozygous plants. The mutant female gametophytes arrested (n = 422) after the first mitosis (two-nucleate stage, 43.1%; Figures 2B and 2C) and less frequently at one-nucleate (1.4%), four-nucleate (3.3%), or later stages (3.0%).

Finally, loss of RRP4 resulted in an additional unique phenotype. Specifically, *rrp4-1* mutant seeds arrested at early stages of embryogenesis (Figures 2D and S4A–S4E). By the time WT progeny seeds of *rrp4-1/RRP4* plants reached the heart or torpedo stages of embryogenesis, 30% of the *rrp4-1/rrp4-1* progeny contained two-cell embryos, 0.5% undivided zygotes, and 3% had embryos at the early globular stage (n = 393). Analysis of stage-specific markers confirmed that *rrp4-1* seed morphology faithfully reflects their developmental timing (Figures S4F and S4G). The *rrp4-1* mutant endosperm developed to varying degrees but never past the cellularization stage (Figures S4B–S4D). These phenotypes cosegregated with the T-DNA genetic lesion, which was confirmed to be a null mutation using an SNP-based assay (Figure 2E), and were fully rescued by the WT and TAP-tagged *RRP4* transgenes. In light of the recent findings that loss of the *Arabidopsis* mRNA decapping complex results in seedling lethality (Goeres et al., 2007; Xu et al., 2006), the phenotype of *rrp4-1* mutant seeds suggests a more general function for RRP4 in postzygotic development, which is consistent with its broad substrate range revealed by tiling microarray analyses (below). In summary, the distinctiveness of the phenotypes of *csl4*, *rrp4*, and *rrp41* mutant plants and their associated molecular signatures (below) indicate that the individual subunits in the *Arabidopsis* exosome core make nonequivalent contributions to its integrity and function. These findings set the plant exosome complex apart from those analyzed so far in other systems.

High-Definition Global Analysis of *Arabidopsis* Exosome Targets

To address the functions of RRP4 and RRP41 during vegetative growth, we engineered an estradiol-inducible RNAi (iRNAi) system (see Experimental Procedures). Growing these transgenic plants on estradiol-containing medium induced the RNAi-mediated knockdown of

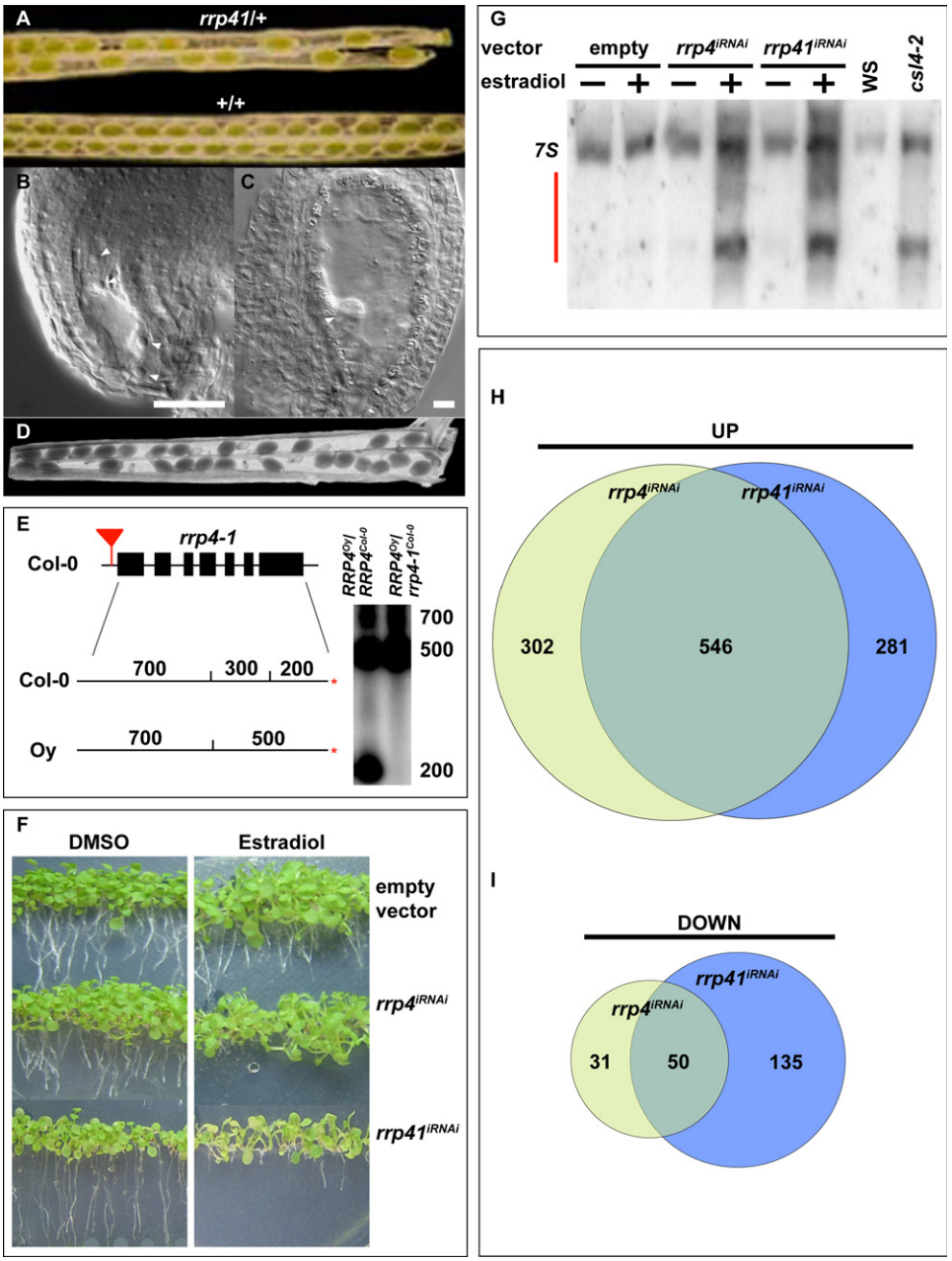

Figure 2. Characterization of the Exosome Mutant Alleles

(A–C) Semisterility (A) and terminal arrest of *rrp41-1* female gametophytes at the four-nuclear stage (B, nuclei are indicated by arrowheads); (C) WT sibling of the female gametophyte shown in (B) has successfully completed development, undergone fertilization, and reached octant stage of embryogenesis (arrowhead, octant embryo). Bar, 50 μm.

(D and E) Embryo lethal phenotype of the *rrp4-1* mutant. (D) *RRP4/rrp4-1* heterozygotes produce normal and aborted seeds in 3:1 ratio. (E) Both Oy and Col-0 alleles are expressed in the WT Col-0/Oy F1 hybrid, but the Col-0-specific SNP is undetectable in the *rrp4-1*$^{Col-0}$/Oy F1. Distal PCR primer was ^{32}P-labeled (asterisk), and RT PCR products digested with HpaII. The *rrp4-1* allele is depicted schematically, and HpaII fragment sizes indicated (in bp).

(F and G) Estradiol-triggered inducible RNAi of RRP4 and RRP41 in seedlings results in growth arrest (F) accompanied by the characteristic defect in processing of the 7S rRNA precursor into mature 5.8S rRNA (G, vertical bar).

(H and I) Venn diagram representation of the up- and down-changes in the *Arabidopsis* transcriptome in response to the depletion of RRP4 and RRP41 by iRNAi.

RRP4 (*rrp4*^{iRNAi}) or *RRP41* (*rrp41*^{iRNAi}) mRNA, resulting in growth arrest (Figure 2F) and subsequent death of seedlings. Importantly, arrest was preceded by accumulation of 3′-underprocessed 5.8S rRNA species (Figure 2G). This molecular phenotype is indicative of exosome malfunction (Mitchell et al., 1997) and was never observed in WT plants exposed to estradiol (neither is growth inhibition). These results show that *Arabidopsis* RRP4 and RRP41 are essential for postembryonic growth and validate the conditional iRNAi knockdown system as a useful approach for investigating their functions in vivo.

To comprehensively identify exosome targets in *Arabidopsis* and gain additional insights into the apparent subfunctionalization of its core subunits, we implemented iRNAi in conjunction with whole-genome tiling microarrays. To minimize changes in gene expression that did not result directly from exosome depletion, we selected the earliest time point of estradiol treatment corresponding to the accumulation of underprocessed 5.8S rRNA species, but before growth retardation. Oligo(dT)-primed targets prepared from RNA samples from plants containing empty vector, *rrp4*^{iRNAi}, or *rrp41*^{iRNAi} constructs grown with or without estradiol were used to interrogate oligonucleotide tiling arrays. Therefore, the array signals should correspond exclusively to polyadenylated RNA species. Moreover, to rule out the possibility of spurious internal priming events, we employed 3′-rapid amplification of cDNA ends (3′-RACE) to map the polyadenylation sites in a subset of targets (Figure S9) as well as compared the relative change in expression between poly(A)$^+$ and total RNA fractions for selected targets (Figures 3C, S5B, S5C, S5H, and S8).

We used the TileMap algorithm, which utilizes a two-state hidden Markov model based on probe-level t statistics (Ji and Wong, 2005), to identify genomic regions showing statistically significant changes. Expression data from arrays hybridized with targets from *rrp4*^{iRNAi} and *rrp41*^{iRNAi} plants that had been estradiol-treated were compared against the corresponding mock (DMSO)-treated samples, as well as against the empty-vector line treated with estradiol. We identified a total of 1612 genomic regions exhibiting increased levels of polyadenylated RNA upon the depletion of RRP4 (*rrp4*^{iRNAi}) and RRP41 (*rrp41*^{iRNAi}), while only about 1/10 as many regions showed downregulation (Figures 2H and 2I; Tables S2 and S3). Depleting an exoribonucleolytic complex should cause increased accumulation of its target RNAs, thus the overwhelming majority of expression changes in RRP4- and RRP41-depleted seedlings most likely represent direct effects.

In contrast, when we conducted a similar analysis of *csl4-2* mutant versus wild-type (Ws) plants, upregulation was no longer a predominant trend (Figure S2). Thus, the constitutive absence of CSL4 likely results in many secondary effects. This observation raises a general concern applicable to transcriptome studies using constitutive loss-of-function mutants and, conversely, emphasizes the value of conditional alleles like *rrp4*^{iRNAi} and *rrp41*^{iRNAi}. At the same time, it is notable that the overlap in the upregulated RNA targets among the *csl4-2*, *rrp4*^{iRNAi}, and *rrp41*^{iRNA} samples is highly significant, while the overlap in spectra of downregulated RNAs is negligible (Figure S2). Hence, the majority of upregulated RNA targets in *csl4-2* seedlings constitute a direct molecular signature of the CSL4-less exosome. Remarkably, many of the exosome targets upregulated in *rrp4*^{iRNAi} and *rrp41*^{iRNAi} samples were unaffected in the *csl4-2* seedlings, including both nuclear-confined species (e.g., miRNA precursors, Figure 5) as well as cytoplasmic RNAs (e.g., spliced mRNAs, Figure 4). Therefore, the CSL4-less exosome is fully active on some of the exosome substrates in both cellular compartments. In addition, these data represent a valuable resource for narrowing down which of the exosome targets are essential for viability, via subtracting the *csl4-2* upregulated dataset from the *rrp4*^{iRNAi} and *rrp41*^{iRNA} analyses. For example, the 7S pre-rRNA processing defect in the *csl4-2* seedlings was as severe as in the RRP4- and RRP41-depleted seedlings (Figure 2G), and yet *csl4-2* mutant plants are phenotypically indistinguishable from WT. A global comparative overview of similarities and differences in the expression changes among the *csl4-2*, *rrp4*^{iRNAi}, and *rrp41*^{iRNA} lines can be found in Figure S2 and Tables S2–S11 and on the accompanying website (http://signal.salk.edu/cgi-bin/exosome).

The following major classes of *Arabidopsis* exosome direct targets were defined by tiling microarray analysis of *rrp4*^{iRNAi} and *rrp41*^{iRNAi} plants: (1) small nuclear RNAs (snRNAs; 9 snRNA genes from both *rrp4*^{iRNAi} and *rrp41*^{iRNAi}; Table S4); (2) the majority of small nucleolar RNAs (snoRNAs) encoded in the genome (83 and 96 snoRNA genes from *rrp4*^{iRNAi} and *rrp41*^{iRNAi} samples, respectively; Table S5); (3) a select subset of tRNA genes (20 and 14, respectively; Table S6); (4) an upregulated subset of *Arabidopsis* mRNAs (205 and 266 mRNAs, respectively; Table S7); (5) a subset of mRNAs that extend beyond their annotated 3′ end, indicative of 3′-processing defects (29 from both *rrp4*^{iRNAi} and *rrp41*^{iRNAi}; Table S8); (6) a subset of specific pri-miRNA genes (12 from *rrp4*^{iRNAi} and 11 from *rrp41*^{iRNAi}; Table S9); (7) a large class of previously uncharacterized noncoding RNAs (ncRNAs); many of these ncRNAs overlap with repetitive elements and small RNA (smRNA)-generating loci (210 and 156 ncRNAs, respectively; Table S10); and (8) a distinct class of previously undetected polyadenylated transcripts that map exclusively to the 5′ ends of known protein-coding mRNAs and hence may possess regulatory potential (52 from both *rrp4*^{iRNAi} and *rrp41*^{iRNAi}; Table S11). Notably, while the overlap in the spectra of upregulated target RNAs revealed by the depletions of RRP4 and RRP41 was highly significant (~64%), the extent of differences between them corroborates the notion of subfunctionalization of the subunits in the *Arabidopsis* exosome core (for example see Figure 4). Taken together, these results circumscribe a complex spectrum of *Arabidopsis* exosome targets that spans RNAP I, II, III, and possibly RNAP IV transcripts and includes nuclear-restricted RNAs (e.g., pri-miRNAs), cytoplasmic RNAs (e.g., spliced mRNAs), as well as RNAs distributed between the two compartments.

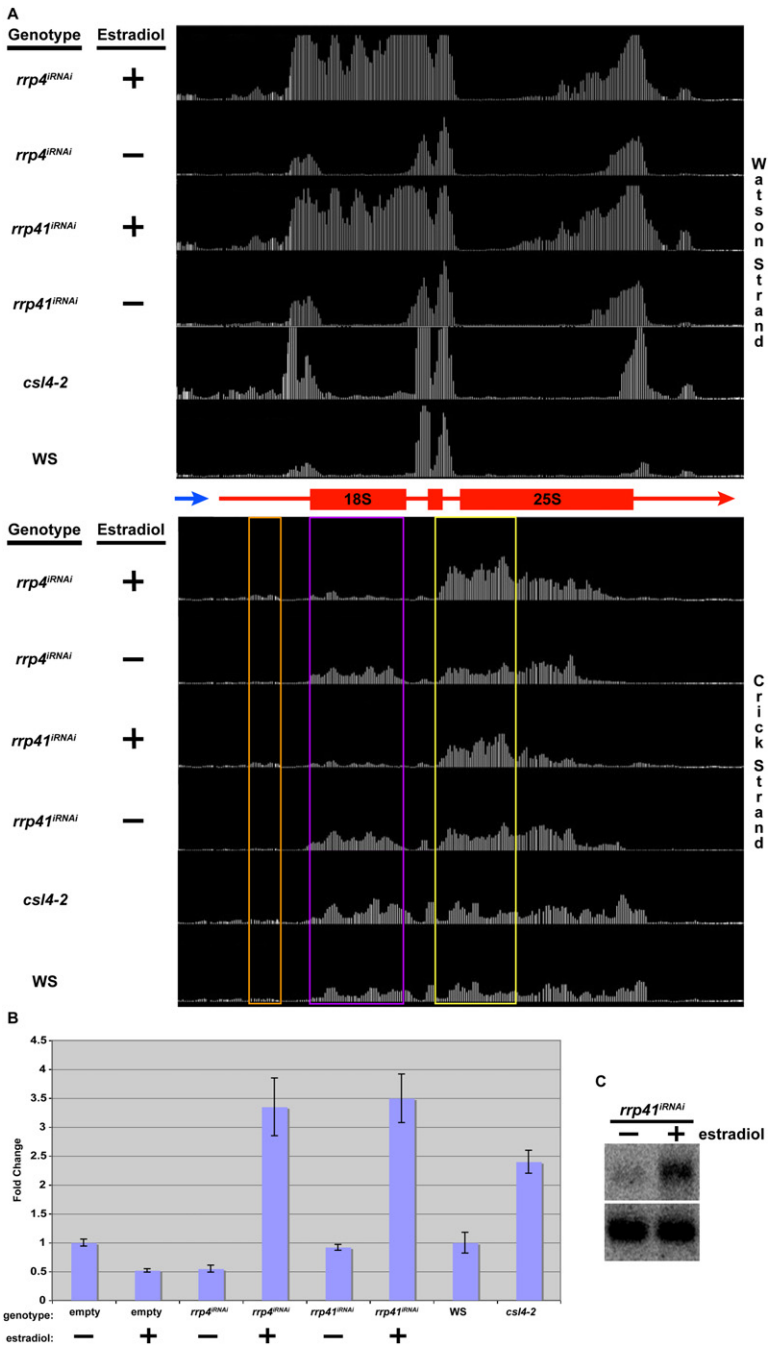

Figure 3. Effect of *Arabidopsis* Exosome Subunits Depletion or Mutation on rRNA Processing

(A) Effects on the sense (Watson strand) and antisense (Crick strand) rRNA-related species. Vertical bars correspond to the array probes. Boxes delimit the boundaries of the regions exhibiting prominent up- (orange and yellow) and down-changes (purple) of antisense rRNA-related transcripts.

(B) RT qPCR validation of upregulation of the IGS transcript (blue arrow in A; error bars, ±SD).

(C) Northern analysis of poly(A)$^+$ (top) and total RNA (bottom) using the same probe as in Figure 2G reveals the accumulation of ~2.4 kb polyadenylated rRNA precursor.

RNA Targets of the *Arabidopsis* Exosome

Stable Structural RNAs

Interestingly, our array analyses identified appreciable amounts of polyadenylated RNA signals across the rDNA repeat unit even under normal conditions, which were dramatically upregulated upon depletion of RRP4 or RRP41 (Figure 3). This increased and expanded signal corresponded largely to polyadenylated pre-rRNA precursors. For example, northern analysis targeting the sequences just downstream of 5.8S rRNA revealed an increase in a polyadenylated, 3′-underprocessed species of ~2.4 kb (Figure 3C, top) that included both the 18S and 5.8S mature rRNA regions, while neither the nonpolyadenylated precursor (Figure 3C, bottom) nor the levels of mature rRNAs (data not shown) were affected. Furthermore, two major clusters of polyadenylation sites identified by 3′-RACE were both located outside of the boundaries of the mature rRNA (Figure S9). These findings parallel observations in yeast, where targeting of pre-rRNA species for degradation by the exosome is mechanistically linked

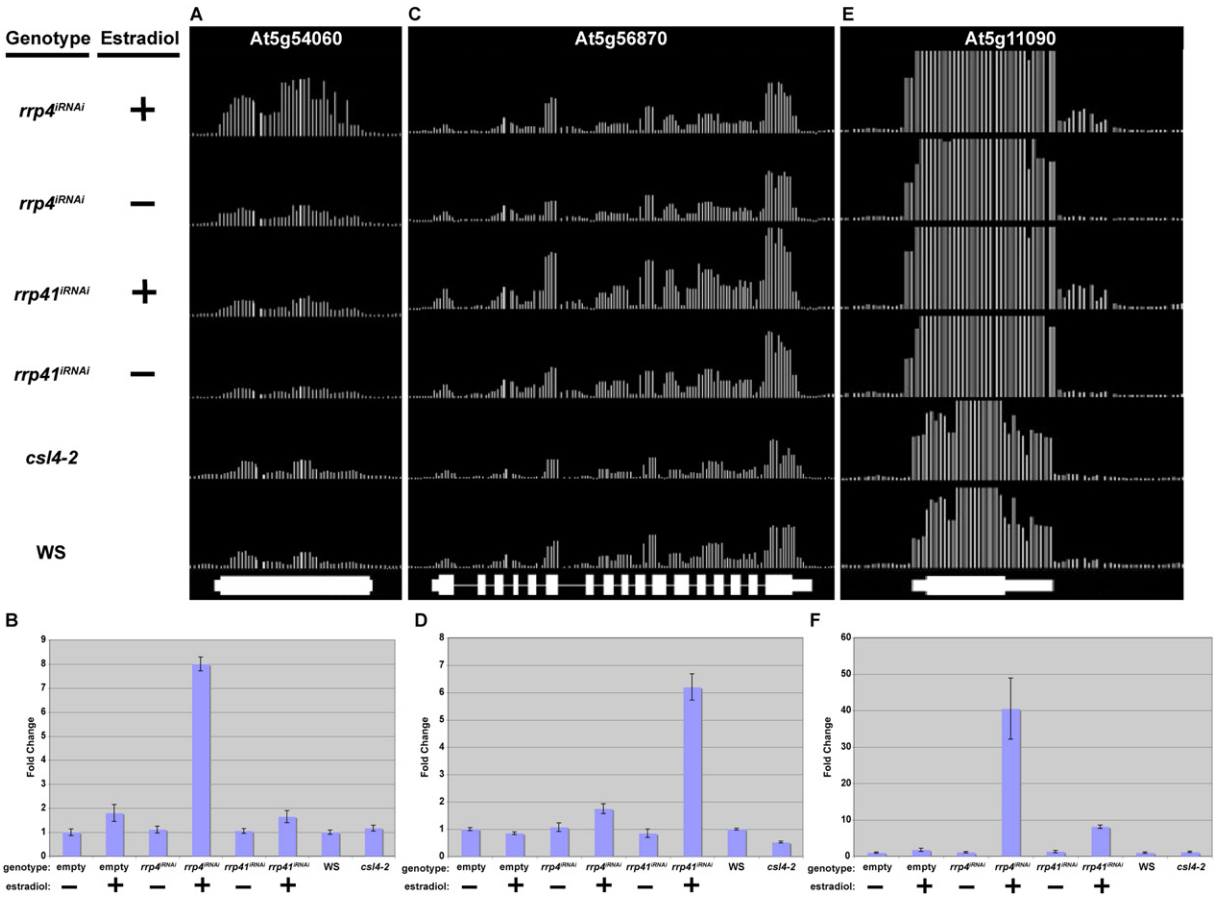

Figure 4. Effects of *Arabidopsis* Exosome Depletion on a Select Subset of mRNA

(A and B) RRP4 depletion-specific upregulation of the glycosyltransferase *At5g54060* mRNA, visualized by tiling microarray hybridization (A) and RT qPCR (B). Error bars, ±SD.

(C and D) RRP41 depletion-specific upregulation of the β-galactosidase *At5g56870* mRNA, visualized by tiling microarray hybridization (C) and RT qPCR (D). Error bars, ±SD.

(E and F) 3′-extension of the *At5g11090* mRNA upon the depletion of either RRP4 or RRP41 exosome subunits, visualized by tiling microarray hybridization (E) and RT qPCR (F). Error bars, ±SD.

to their oligoadenylation by the TRAMP complex (Kadaba et al., 2004; Vanacova et al., 2005).

In addition, both tiling array and qPCR analyses revealed increased accumulation of poly(A)$^+$ RNAs in the intergenic spacer region (IGS, Figures 3A and 3B). Notably, in mouse cells the IGS-derived RNA regulates the activity of the main rDNA promoter in an epigenetically stable manner (Mayer et al., 2006). Interestingly, depletion of RRP4 and RRP41 also impacted the abundance of polyadenylated RNAs of antisense polarity relative to rRNAs. For example, we observed a strong increase in transcripts complementary to the external transcribed spacer and to the 5′ half of 25S rRNA. Conversely, exosome depletion led to the significant decrease of a naturally occurring antisense RNA whose boundaries closely correspond to that of 18S rRNA. Notably, this polyadenylated antisense RNA is immediately flanked by polyadenylated sense RNA, suggestive of a mutually exclusive relationship. Moreover, in *csl4-2* seedlings, where the upregulation of the sense poly(A)$^+$ RNA in the 18S region does not occur, this antisense species is not downregulated (Figure 3A). Therefore, these findings may be indicative that rRNA C-related species are regulated by complementary antisense transcripts.

Tiling array data also revealed that depletion of RRP4 and RRP41 resulted in dramatic increases in accumulation of poly(A)$^+$ snRNAs (Table S4) and snoRNAs (Table S5), including those encoded by free-standing polycistronic clusters (Figures S5A–S5C), solitary genes (Figure S8A), as well as those embedded in introns of genes functionally related to protein synthesis (Table S5). The latter gene arrangement may help to coordinate snoRNA biogenesis with cellular demands on translation and is prevalent in animals, but it has been observed in *Arabidopsis* only once (Barneche et al., 2000). Moreover, we identified 3′-extended upregulated poly(A)$^+$ snoRNAs (Figures S5A and

S5B), which may represent either incompletely processed byproducts of snoRNA biogenesis targeted for degradation or normal processing intermediates.

Several classes of *Arabidopsis* small stable RNAs constitute previously unknown exosome substrates. One example is the RNAP III-transcribed *MRP/7-2* RNA (Figures S4E and S4F), which in yeast is processed by Rex3, not the exosome (van Hoof et al., 2000). Second, we observed accumulation of a poly(A)$^+$ form, as well as of the 3′-extended species of 7SL RNA, also an RNAP III transcript (Figures S5G–S5I and S9). Hence, the *Arabidopsis* exosome may degrade the poly(A)$^+$ 7SL RNA during RNA quality control and/or process 3′-readthrough species into mature 7SL RNA. Notably, the scattered distribution of polyadenylation sites throughout the RNA body in MRP, 7SL, U12, and U3B RNAs (Figure S9) is consistent with repeated cycles of oligoadenylation by TRAMP and exosomal "nibbling" (LaCava et al., 2005; Vanacova et al., 2005; Wyers et al., 2005). Third, we observed strong accumulation of a poly(A)$^+$ tRNA^{Tyr} (Figure S5D; Table S6), which is different from the tRNA species downregulated by the exosome and TRAMP in yeast (Kadaba et al., 2004). Biogenesis of plant tRNA^{Tyr} requires highly ordered events of $U_{35} \rightarrow \psi_{35}$ modification and splicing (Akama et al., 1997), hence this observation likely reflects the role of the exosome in proofreading of this complex process. Taken together, our observations of massive accumulation in exosome-depleted seedlings of poly(A)$^+$ forms of many stable RNAs strongly suggest that oligoadenylation coupled to exosome-mediated RNA quality control and/or processing are fundamental features of plant gene expression.

Messenger RNAs

The exosome degrades poly(A)$^-$ intermediates of mRNA decay produced by deadenylating enzymes. Poly(A)$^-$ species cannot be detected in microarray experiments using oligo(dT)-primed targets. Nevertheless, a number of upregulated signals detected in the exosome-depleted *Arabidopsis* seedlings were protein-coding mRNAs (Table S7). Notably, transcripts from intronless genes were highly overrepresented in this category ($p < 0.001$), suggesting a significant enrichment for processed pseudogenes. Moreover, a surprising proportion of the upregulated regions were of antisense polarity (23.3% for *rrp41^{iRNAi}* and 24.4% for *rrp4^{iRNAi}*). These findings suggest that sense and antisense poly(A)$^+$ transcripts derived from potential pseudogenes in *Arabidopsis* are specifically and directly targeted for exosome-mediated 3′–5′ decay.

Interestingly, a number of mRNAs targeted by the *Arabidopsis* exosome exhibit subunit-specific responses (Table S7). For example, the level of a putative glycosyltransferase mRNA (*At5g54060*) is increased upon the depletion of RRP4 but not of RRP41, while the opposite is true for a putative β-galactosidase mRNA (*At5g56870*; Figures 4A–4D). While the mechanistic basis of differential sensitivity to the depletion of RRP4 or RRP41 remains to be determined, these examples parallel their distinct mutant phenotypes and corroborate the notion of subfunctionalization of the *Arabidopsis* exosome core subunits.

Unexpectedly, tiling array experiments also revealed a number of mRNAs with extended 3′ ends but whose absolute levels were unaffected (Table S8; Figures 4E and 4F). This may be indicative of *Arabidopsis* exosome-mediated degradation of aberrant readthrough mRNAs although we cannot rule out the alternative possibility that the exosome participates in 3′ end formation of some mRNAs.

Intermediates of microRNA Biogenesis

Depletion of RRP4 and RRP41 also revealed significant increases in pri-miRNA transcripts (Table S9; Figure 5). Interestingly, the increased signal was mostly located upstream of the stem-loop structure that harbors the miRNA/miRNA* duplex, while the downstream segments were usually unaffected (Figure 5A), and the levels of mature miRNAs were also unchanged (Figure 5C). In addition, our analyses revealed novel polyadenylated intermediates corresponding to the region between the miRNA and miRNA* (Figures 5D, S6B, and S9). Together, these findings delineate a 3′–5′ pathway of removal of upstream and middle (loop) byproducts involving TRAMP-like and exosome activities (Figure S6A). Although these exosome-dependent reactions do not appear rate limiting for biogenesis of mature miRNAs, they likely facilitate efficient recycling of the pre-miRNA processing factors. Surprisingly, our 3′-RACE analyses of the upregulated signal in the pri-miRNA168a transcript demonstrated that in the majority of cases (72%) polyadenylation occurred immediately upstream of the mature miRNA sequence (Figures 5B and S6C), indicating that pri-miRNA168a is often cleaved directly at the precursor/miRNA boundary. These findings are inconsistent with the proposed two-step pathway of plant miRNA biogenesis via an initial processing of pri-miRNA into pre-miRNA, followed by processing of pre-miRNA into mature miRNA (Kurihara and Watanabe, 2004), and suggest the existence of possible alternative pathways.

Heterochromatic Repeat-Associated and Novel Noncoding RNAs

Additionally, tiling microarray experiments revealed the accumulation of numerous poly(A)$^+$ transcripts that have neither protein-coding potential nor predicted functions. Significantly, a large fraction of these RNA species escaped detection in previous transcriptome analyses (Meyers et al., 2004; Yamada et al., 2003), apparently because their steady-state levels in WT plants are tightly downregulated via exosome-mediated degradation (Table S10). Notably, there was a highly significant overlap among these RNAs in *rrp4^{iRNAi}*, *rrp41^{iRNAi}*, and *csl4-2* samples (Figure S2C). Remarkably, these novel exosome-specific RNAs exhibit a strikingly nonrandom association with small RNA-producing loci, as well as with repeated sequences: 72% from *rrp4^{iRNAi}* and 63% from *rrp41^{iRNAi}* ($p < 0.001$; Figures 6A and 6B). Furthermore, we often observed the accumulation of complementary RNAs of both polarities (Figures 6C and 6E). Another characteristic

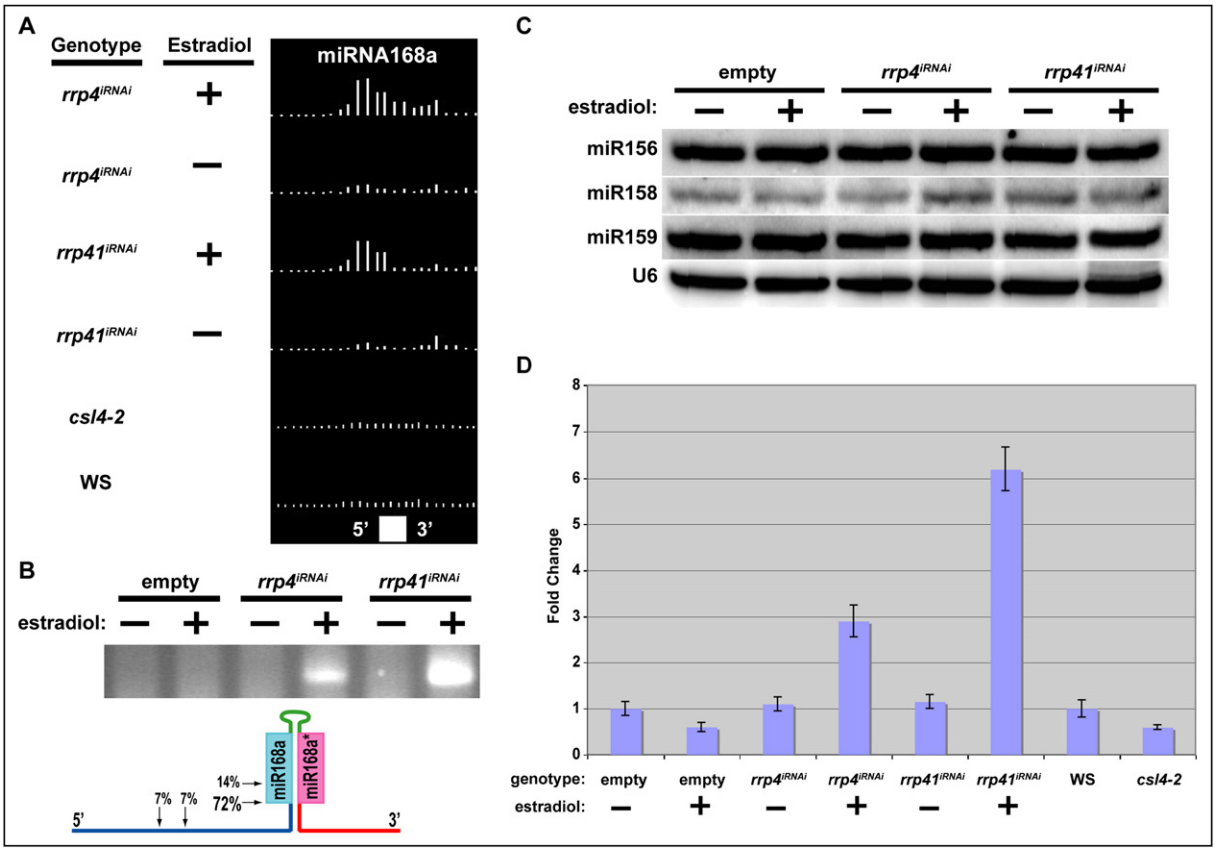

Figure 5. Effects of Exosome Subunit Depletion on pri-miRNA Processing Intermediates

(A) Tiling microarray data demonstrating upregulated poly(A)$^+$ RNA for the pri-miR168a gene upstream of the mature miRNA sequence.

(B) 3′-RACE of pri-miRNA168a; distribution of 3′-endpoints of the sequenced 3′-RACE products are shown in the bottom panel.

(C) Northern blot analysis demonstrates that mature miRNA levels are not affected by exosome depletion.

(D) Oligo(dT)-primed RT qPCR targeting the loop region of pre-miR156e. Error bars, ±SD.

example concerns an exosome-specific sense/antisense transcript pair emanating from a repetitive sequence element containing 42 bp interspersed tandem subrepeats (Figure 6G). Such sense/antisense transcript pairs serve as precursors for the ~24 nt endogenous heterochromatic small-interfering RNAs (siRNAs) that guide RNA-dependent DNA methylation (RdDM) and H3K9 methylation of transposon and tandem repeat loci (Cao et al., 2003; Lippman and Martienssen, 2004; Xie et al., 2004; Zilberman et al., 2004). Therefore, we confirmed the increased expression of the 5S rDNA region that gives rise to siRNA1003 in RRP4- and RRP41-depleted seedlings, as well as *csl4-2* mutant plants (mature 5S rRNA levels were unaffected; Figures 6C and 6D). Notably, the novel exosome-specific ncRNAs are preferentially associated with centromeric and pericentromeric regions of the *Arabidopsis* genome highly coincident with repetitive elements and DNA methylation (Zhang et al., 2006), while exosome-regulated mRNAs are excluded from these regions (Figure 6H). Hence, the *Arabidopsis* exosome may have a general role in quality control of RdDM-associated siRNA biogenesis precursors and/or degrade heterochromatin-associated RNAs, as shown for heterochromatic silencing of select loci in *S. pombe* (Bühler et al., 2007). Overall, these data suggest that the *Arabidopsis* exosome plays an important role in regulating heterochromatin-associated transcripts.

Another remarkable example of a novel ncRNA upregulated upon exosome knockdown was an ~4 kb long transcript lacking significant protein-coding capacity but conserved in closely related dicots (e.g., *Capsella rubella*, Figures 7A–7C). Curiously, sequence conservation between the *Arabidopsis* and *Capsella* transcripts is confined to two interspersed short direct repeats 16 nt and 24 nt in length (Figures 7B and S7), suggesting that these small conserved segments constitute its functionally important elements. For example, they might serve as recognition sites for RNA-binding proteins or be processed out to form small RNAs. These repeated segments do not reside in secondary structures resembling DICER substrates, thus their processing would likely have a distinct mechanistic basis.

Perhaps the most intriguing category of exosome targets was a distinct subclass of ncRNAs colinear with the

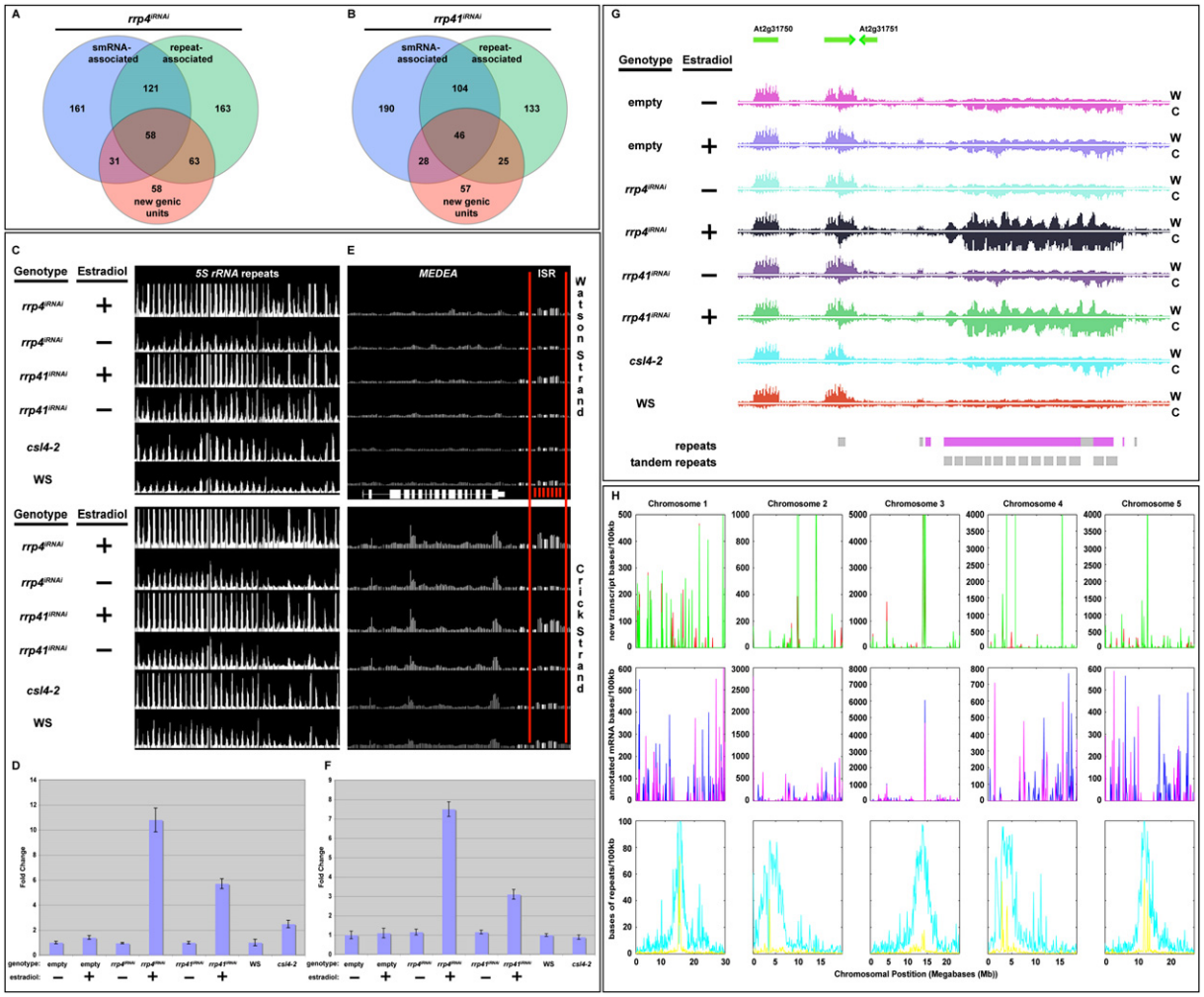

Figure 6. Effects of Exosome Subunit Depletion or Mutation on Novel Transcripts Associated with siRNAs and Repetitive Elements

(A and B) Venn diagram representation of upregulated, exosome-specific transcripts and their highly significant association with smRNA-generating loci and repetitive elements. As shown in the Venn diagrams, the majority of transcripts that are only observed upon exosome depletion are associated with smRNA-generating loci and/or repetitive elements (72% for *rrp4*^{iRNAi} and 63% for *rrp41*^{iRNAi} lines).

(C–F) Upregulation of transcripts encoded on both strands of tandem repeats. (C and D) Polyadenylated 5S transcripts: (C) tiling microarray data, (D) RT qPCR results. Note the 500 bp periodicity in the tandem repeat signals in (C). (E and F) Polyadenylated transcripts from the MEA-ISR repeats (red boxes). Error bars, ±SD.

(G) An example of an upregulated, exosome-specific transcript (screenshot from the exosome-regulated transcriptome database, http://signal.salk.edu/cgi-bin/exosome). W and C indicate signal from Watson and Crick strands of the *Arabidopsis* genome. Repetitive element is denoted by purple bar, with its constituent 42 bp tandem repeats indicated by the dark gray boxes.

(H) Chromosomal distribution of novel upregulated, exosome-specific transcripts. Top panels demonstrate the total length of novel upregulated, exosome-specific transcripts (*y* axis, left-side scale) in a sliding 100 kb window in *rrp4*^{iRNAi} (green line) and *rrp41*^{iRNAi} (red line) treated with estradiol. Middle panels show the total length of annotated mRNAs upregulated upon estradiol treatment of *rrp4*^{iRNAi} (purple line) and *rrp41*^{iRNAi} (blue line) plants. Bottom panels demonstrate the total lengths of all repeats (light blue line) and tandem repeats (yellow line) in a sliding 100 kb window.

5′ ends of known protein-coding transcripts (Table S11 and Figures 7D and 7E). We propose that the origin of these ncRNAs (hereafter called upstream noncoding transcripts, or UNTs) is distinct from that of the overlapping "main" RNAP II transcription units. First, they are unlikely to be derived from cytoplasmic mRNA degradation because the exosome enters the decay pathway after mRNA deadenylation and degrades the mRNA body processively in a 3′–5′ direction. Hence, exosome depletion would cause an accumulation of deadenylated, full-length transcripts and/or heterogeneous populations of 3′-truncated poly(A)$^-$ fragments with endpoints scattered throughout the mRNA body (Anderson and Parker, 1998). In contrast, the UNTs are collinear only with the 5′ ends of known mRNAs (Figure S9). Also, UNTs frequently extend into the first intron of respective overlapping genes. The possibility that UNTs derive from the pre-mRNAs is highly improbable, particularly when the UNT

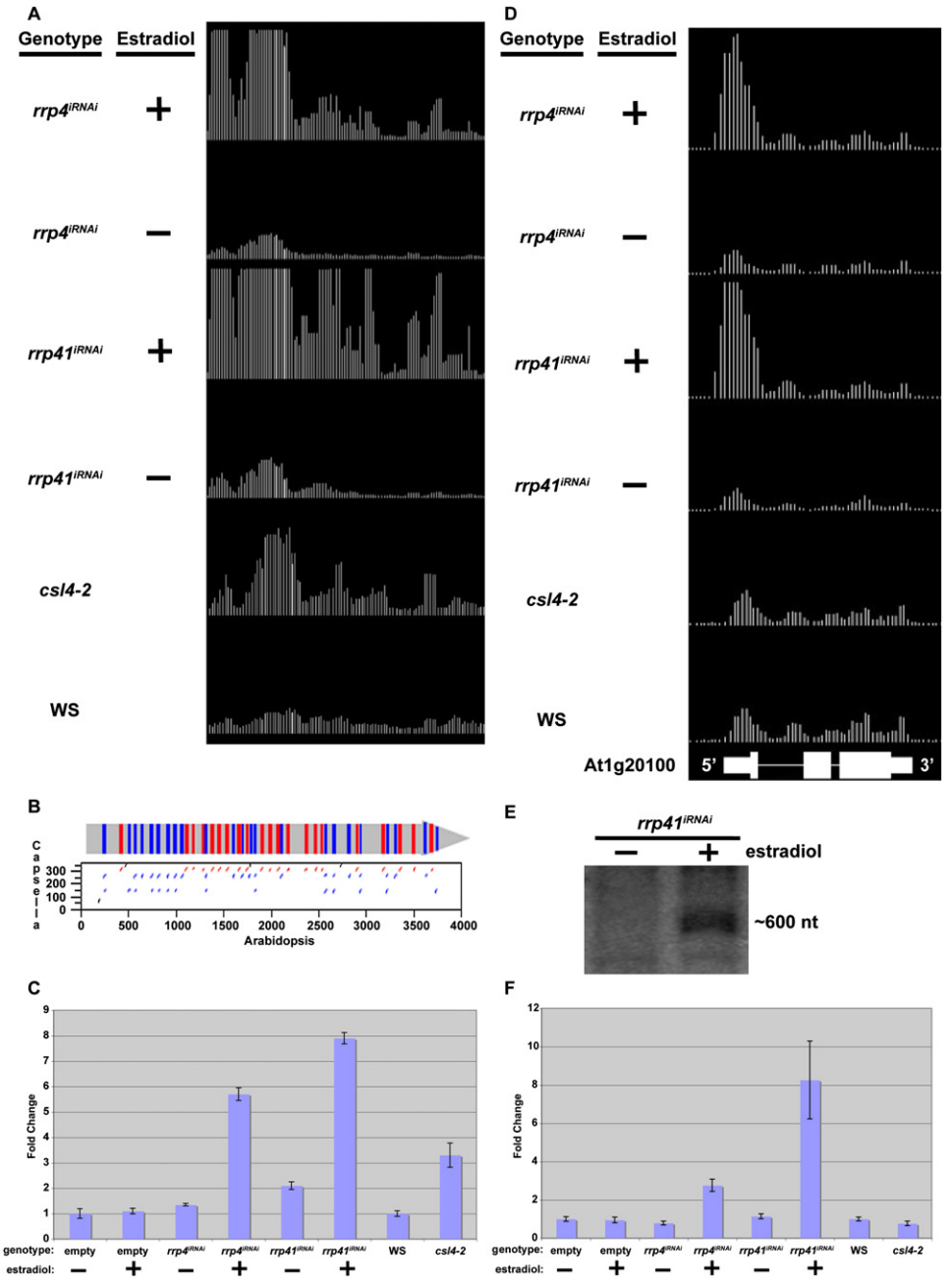

Figure 7. Examples of Novel Noncoding RNAs Revealed by Tiling Microarray Analyses of *Arabidopsis* Exosome Depletion

(A–C) Upregulation of a ~4 kb long transcript containing internal short interspersed repeats conserved in *Capsella rubella*. (A) Tiling microarray data. (B) Schematic of the transcript and a dotplot of the *Arabidopsis*/*Capsella* alignment, with the two classes of interspersed internal repeats color-coded in blue and red. (C) Results of the RT qPCR. Error bars, ±SD.

(D and E) Example of the strongly upregulated upstream noncoding transcript (UNT) in the 5' region of *At1g20100* in the exosome subunit-depleted seedlings. (D) Tiling microarray data. (E) Northern blot analysis of poly(A)$^+$ RNA.

(F) Results of the RT qPCR. Error bars, ±SD.

is more abundant than the corresponding mRNA (Figures 7D and 7E).

The striking association of *Arabidopsis* UNTs with the 5′ ends of RNAP II transcription units must reflect some aspect of their biogenesis or function. Several features of UNTs are reminiscent of cryptic unstable transcripts (CUTs) in yeast, which are present at very low levels in WT cells (Wyers et al., 2005). CUTs are frequently associated with promoters of protein-coding genes, and while some may merely reflect transcriptional noise, others

may also have biological functions (Davis and Ares, 2006; Kopcewicz et al., 2007). Moreover, recent detailed mapping of the human transcriptome also revealed an abundant class of promoter-associated short (up to 200 nt) ncRNAs, termed PASRs (Kapranov et al., 2007), which also may act as negative regulators of the main transcription units (Martianov et al., 2007). Although UNTs may differ from both CUTs and PASRs because their 5′ ends appear to coincide with those of the main RNAP II transcripts (Figures 7D and S9), our results suggest that the exosome-regulated ncRNAs associated with 5′ ends of genes likely represent a fundamental regulatory feature of eukaryotic transcriptomes.

Conclusion

We combined genetic, proteomic, and whole-transcriptome analyses to investigate the function of the exosome complex in the multicellular eukaryote *Arabidopsis thaliana*. We find that individual subunits of the plant exosome are functionally specialized, ranging from being dispensable for growth and development (CSL4) to being essential for the development of female gametophytes (RRP41) or embryogenesis (RRP4). Moreover, the plant exosome complex lacking its CSL4 subunit is partially intact and functional. These findings demonstrate an unexpected degree of functional plasticity in the plant exosome core. Our whole-genome tiling array analyses revealed numerous novel exosome substrates, new metabolic aspects of several known important RNA species, a broad role of the exosome in regulation of ncRNAs associated with heterochromatic regions, as well as the widespread occurrence of polyadenylation- and exosome-mediated RNA quality control in plants. Furthermore, our findings reveal a "deeply hidden" layer of the transcriptome composed of intergenic noncoding transcripts that are tightly downregulated by constitutive exosome activity. Finally, a publicly available exosome-regulated transcriptome database (http://signal.salk.edu/cgi-bin/exosome) should aid in illuminating new fundamental components and regulatory mechanisms in complex eukaryotic transcriptomes.

EXPERIMENTAL PROCEDURES

Plant Material and Reverse Genetics

Mutant alleles *csl4-1* and *csl4-2* correspond to SALK_004561 (Alonso et al., 2003) and FLAG_055B05 lines, respectively. The *rrp4-1* allele is SALK_025995, *rrp41-2* and *rrp41-3* are SALK_139189 and SALK_112819, respectively, while *rrp41-1* was isolated from the University of Wisconsin BASTA population. WT plants of matching accessions were used in all reciprocal crosses (Col-0 for all Salk alleles and Ws for FLAG and University of Wisconsin alleles). For complementation with the WT and TAP tagged transgenes, respective heterozygotes were transformed (Clough and Bent, 1998) and the progeny plants lacking the WT allele and containing both the T-DNA insertion allele and the transgene identified by PCR.

Proteomics

TAP purification protocol was adapted from Rigaut et al. (1999). The Coomassie-stained protein bands were treated with trypsin using an In-Gel Digestion kit (Pierce), and dried peptides dissolved in 50% acetonitrile, 0.1% trifluoroacetic acid with 5 mg/ml alpha 4-hydroxycinnamic acid as a matrix. 0.6 μl of peptide/matrix mix was loaded onto the 6AB MALDI sample plate, dried, and subjected to MALDI-TOF MS and subsequent MS/MS analyses using the 4700 Proteomics Analyzer and GPS software (Applied BioSystems). A combination of peptide mass fingerprinting (PMF) and MS/MS sequencing analysis was performed using the Mascot search engine. Fragmentation of the precursors was carried out using the collision-induced dissociation (CID). CID spectra were submitted for protein identifications with a precursor precision tolerance of 1 Da and MS/MS fragment tolerance of 0.5 Da. A criterion of correct protein identification was a confidence interval exceeding 95%, which was a combination of protein scores from PMF and ion scores from MS/MS sequencing.

Inducible RNAi

RNAi cassettes contained 940 bp (*RRP4*) or 788 bp (*RRP41*) fragments of the target cDNA sequence as a pair of inverted repeats, separated by the *FAD2* intron in the pER8 vector backbone (Zuo et al., 2000). For iRNAi, seedlings were germinated and grown for ≤7 days on 8 μM of 17β-estradiol.

RNA Analyses

Polyacrylamide Northern blot analyses were performed as described (Chekanova et al., 2000). Transcripts were quantified by RT qPCR using the comparative threshold cycle method ($\Delta\Delta C_t$, primers listed in Table S16), using Actin 3 (At3g53750) as endogenous reference.

RNA Extraction, Probe Synthesis, Microarray Hybridization, and Analysis

Fifteen micrograms of total RNA extracted using TRIzol (Invitrogen) was used to synthesize double-stranded cDNA using the GeneChip One-Cycle cDNA Synthesis Kit (Affymetrix). Biotin-labeled cRNA was generated using the GeneChip IVT Labeling Kit and fragmented, and 15 μg of cRNA was hybridized to *Arabidopsis* tiling arrays (Zhang et al., 2006). Hybridization, staining, and washing were performed according to the Affymetrix Eukaryotic Target Protocol. A minimum of two biological replicates were performed for each of the three genotypes, the empty vector (referred to as WT for brevity), $rrp4^{iRNAi}$, and $rrp41^{iRNAi}$, using estradiol or control (DMSO) treatment. The TileMap tiling array analysis software package (Ji and Wong, 2005) was used to detect statistically significant differences in transcriptional activity in the tiling microarray data as described in Zhang et al. (2006) and further detailed in the Supplemental Data.

Supplemental Data

Supplemental Data include Experimental Procedures, nine figures, and eighteen tables and can be found with this article online at http://www.cell.com/cgi/content/full/131/7/1340/DC1/.

ACKNOWLEDGMENTS

This research was supported by grants from the USDA (2005-35301-15757) and the National Science Foundation (MCB-0424651) to D.A.B. and DBI-0520253 and DBI-0420126 to J.R.E. B.D.G. is a Damon Runyon Fellow supported by the Damon Runyon Cancer Research Foundation (DRG-1909-06). We thank Tarik El-Mellouki, Karim Pirani, Mark Urich, and Megan Hatlen for technical assistance and Kim Emerson for artwork.

Received: June 27, 2007
Revised: October 1, 2007
Accepted: October 25, 2007
Published: December 27, 2007

REFERENCES

Akama, K., Nass, A., Junker, V., and Beier, H. (1997). Characterization of nuclear tRNA(Tyr) introns: their evolution from red algae to higher plants. FEBS Lett. *417*, 213–218.

Allmang, C., Kufel, J., Chanfreau, G., Mitchell, P., Petfalski, E., and Tollervey, D. (1999a). Functions of the exosome in rRNA, snoRNA and snRNA synthesis. EMBO J. *18*, 5399–5410.

Allmang, C., Petfalski, E., Podtelejnikov, A., Mann, M., Tollervey, D., and Mitchell, P. (1999b). The yeast exosome and human PM-Scl are related complexes of 3′–> 5′ exonucleases. Genes Dev. *13*, 2148–2158.

Allmang, C., Mitchell, P., Petfalski, E., and Tollervey, D. (2000). Degradation of ribosomal RNA precursors by the exosome. Nucleic Acids Res. *28*, 1684–1691.

Alonso, J.M., Stepanova, A.N., Leisse, T.J., Kim, C.J., Chen, H., Shinn, P., Stevenson, D.K., Zimmerman, J., Barajas, P., Cheuk, R., et al. (2003). Genome-wide insertional mutagenesis of Arabidopsis thaliana. Science *301*, 653–657.

Anderson, J.S., and Parker, R.P. (1998). The 3′ to 5′ degradation of yeast mRNAs is a general mechanism for mRNA turnover that requires the SKI2 DEVH box protein and 3′ to 5′ exonucleases of the exosome complex. EMBO J. *17*, 1497–1506.

Baker, R.E., Harris, K., and Zhang, K. (1998). Mutations synthetically lethal with cep1 target S. cerevisiae kinetochore components. Genetics *149*, 73–85.

Barneche, F., Steinmetz, F., and Echeverria, M. (2000). Fibrillarin genes encode both a conserved nucleolar protein and a novel small nucleolar RNA involved in ribosomal RNA methylation in *Arabidopsis thaliana*. J. Biol. Chem. *275*, 27212–27222.

Bousquet-Antonelli, C., Presutti, C., and Tollervey, D. (2000). Identification of a regulated pathway for nuclear pre-mRNA turnover. Cell *102*, 765–775.

Brouwer, R., Allmang, C., Raijmakers, R., van Aarssen, Y., Egberts, W.V., Petfalski, E., van Venrooij, W.J., Tollervey, D., and Pruijn, G.J. (2001). Three novel components of the human exosome. J. Biol. Chem. *276*, 6177–6184.

Bühler, M., Haas, W., Gygi, S.P., and Moazed, D. (2007). RNAi-dependent and -independent RNA turnover mechanisms contribute to heterochromatic gene silencing. Cell *129*, 707–721.

Cao, X., Aufsatz, W., Zilberman, D., Mette, M.F., Huang, M.S., Matzke, M., and Jacobsen, S.E. (2003). Role of the DRM and CMT3 methyltransferases in RNA-directed DNA methylation. Curr. Biol. *13*, 2212–2217.

Chekanova, J.A., Shaw, R.J., Wills, M.A., and Belostotsky, D.A. (2000). Poly(A) tail-dependent exonuclease AtRrp41p from Arabidopsis thaliana rescues 5.8 S rRNA processing and mRNA decay defects of the yeast ski6 mutant and is found in an exosome-sized complex in plant and yeast cells. J. Biol. Chem. *275*, 33158–33166.

Chekanova, J.A., Dutko, J.A., Mian, I.S., and Belostotsky, D.A. (2002). Arabidopsis thaliana exosome subunit AtRrp4p is a hydrolytic 3′→5′ exonuclease containing S1 and KH RNA-binding domains. Nucleic Acids Res. *30*, 695–700.

Chen, C.Y., Gherzi, R., Ong, S.E., Chan, E.L., Raijmakers, R., Pruijn, G.J., Stoecklin, G., Moroni, C., Mann, M., and Karin, M. (2001). AU binding proteins recruit the exosome to degrade ARE-containing mRNAs. Cell *107*, 451–464.

Clough, S.J., and Bent, A.F. (1998). Floral dip: a simplified method for Agrobacterium-mediated transformation of Arabidopsis thaliana. Plant J. *16*, 735–743.

Das, B., Butler, J.S., and Sherman, F. (2003). Degradation of normal mRNA in the nucleus of Saccharomyces cerevisiae. Mol. Cell. Biol. *23*, 5502–5515.

Davis, C.A., and Ares, M., Jr. (2006). Accumulation of unstable promoter-associated transcripts upon loss of the nuclear exosome subunit Rrp6p in Saccharomyces cerevisiae. Proc. Natl. Acad. Sci. USA *103*, 3262–3267.

Dziembowski, A., Lorentzen, E., Conti, E., and Seraphin, B. (2007). A single subunit, Dis3, is essentially responsible for yeast exosome core activity. Nat. Struct. Mol. Biol. *14*, 15–22.

Estevez, A.M., Kempf, T., and Clayton, C. (2001). The exosome of Trypanosoma brucei. EMBO J. *20*, 3831–3839.

Estevez, A.M., Lehner, B., Sanderson, C.M., Ruppert, T., and Clayton, C. (2003). The roles of intersubunit interactions in exosome stability. J. Biol. Chem. *278*, 34943–34951.

Goeres, D.C., Van Norman, J.M., Zhang, W., Fauver, N.A., Spencer, M.L., and Sieburth, L.E. (2007). Components of the Arabidopsis mRNA decapping complex are required for early seedling development. Plant Cell *19*, 1549–1564.

Graham, A.C., Kiss, D.L., and Andrulis, E.D. (2006). Differential distribution of exosome subunits at the nuclear lamina and in cytoplasmic foci. Mol. Biol. Cell *17*, 1399–1409.

Hooker, T.S., Lam, P., Zheng, H., and Kunst, L. (2007). A core subunit of the RNA-processing/degrading exosome specifically influences cuticular wax biosynthesis in Arabidopsis. Plant Cell *19*, 904–913.

Houalla, R., Devaux, F., Fatica, A., Kufel, J., Barrass, D., Torchet, C., and Tollervey, D. (2006). Microarray detection of novel nuclear RNA substrates for the exosome. Yeast *23*, 439–454.

Houseley, J., LaCava, J., and Tollervey, D. (2006). RNA-quality control by the exosome. Nat. Rev. Mol. Cell Biol. *7*, 529–539.

Ji, H., and Wong, W.H. (2005). TileMap: create chromosomal map of tiling array hybridizations. Bioinformatics *21*, 3629–3636.

Kadaba, S., Krueger, A., Trice, T., Krecic, A.M., Hinnebusch, A.G., and Anderson, J. (2004). Nuclear surveillance and degradation of hypomodified initiator tRNAMet in S. cerevisiae. Genes Dev. *18*, 1227–1240.

Kadaba, S., Wang, X., and Anderson, J.T. (2006). Nuclear RNA surveillance in Saccharomyces cerevisiae: Trf4p-dependent polyadenylation of nascent hypomethylated tRNA and an aberrant form of 5S rRNA. RNA *12*, 508–521.

Kapranov, P., Cheng, J., Dike, S., Nix, D.A., Duttagupta, R., Willingham, A.T., Stadler, P.F., Hertel, J., Hackermueller, J., Hofacker, I.L., et al. (2007). RNA maps reveal new RNA classes and a possible function for pervasive transcription. Science *316*, 484–488.

Kopcewicz, K.A., O'Rourke, T.W., and Reines, D. (2007). Metabolic regulation of IMD2 transcription and an unusual DNA element that generates short transcripts. Mol. Cell. Biol. *27*, 2821–2829.

Kurihara, Y., and Watanabe, Y. (2004). Arabidopsis micro-RNA biogenesis through Dicer-like 1 protein functions. Proc. Natl. Acad. Sci. USA *101*, 12753–12758.

LaCava, J., Houseley, J., Saveanu, C., Petfalski, E., Thompson, E., Jacquier, A., and Tollervey, D. (2005). RNA degradation by the exosome is promoted by a nuclear polyadenylation complex. Cell *121*, 713–724.

Libri, D., Dower, K., Boulay, J., Thomsen, R., Rosbash, M., and Jensen, T.H. (2002). Interactions between mRNA export commitment, 3′-end quality control, and nuclear degradation. Mol. Cell. Biol. *22*, 8254–8266.

Lippman, Z., and Martienssen, R. (2004). The role of RNA interference in heterochromatic silencing. Nature *431*, 364–370.

Liu, Q., Greimann, J.C., and Lima, C.D. (2006). Reconstitution, activities, and structure of the eukaryotic RNA exosome. Cell *127*, 1223–1237.

Liu, Q., Greimann, J.C., and Lima, C.D. (2007). Erratum: Reconstitution, activities, and structure of the eukaryotic RNA exosome. Cell *131*, 188–190.

Martianov, I., Ramadass, A., Serra Barros, A., Chow, N., and Akoulitchev, A. (2007). Repression of the human dihydrofolate reductase gene by a non-coding interfering transcript. Nature *445*, 666–670.

Mayer, C., Schmitz, K.M., Li, J., Grummt, I., and Santoro, R. (2006). Intergenic transcripts regulate the epigenetic state of rRNA genes. Mol. Cell *22*, 351–361.

Meyers, B.C., Vu, T.H., Tej, S.S., Ghazal, H., Matvienko, M., Agrawal, V., Ning, J., and Haudenschild, C.D. (2004). Analysis of the transcriptional complexity of Arabidopsis thaliana by massively parallel signature sequencing. Nat. Biotechnol. *22*, 1006–1011.

Mitchell, P., Petfalski, E., Shevchenko, A., Mann, M., and Tollervey, D. (1997). The exosome: a conserved eukaryotic RNA processing complex containing multiple 3′→5′ exoribonucleases. Cell *91*, 457–466.

Mitchell, P., Petfalski, E., Houalla, R., Podtelejnikov, A., Mann, M., and Tollervey, D. (2003). Rrp47p is an exosome-associated protein required for the 3′ processing of stable RNAs. Mol. Cell. Biol. *23*, 6982–6992.

Peng, W.T., Robinson, M.D., Mnaimneh, S., Krogan, N.J., Cagney, G., Morris, Q., Davierwala, A.P., Grigull, J., Yang, X., Zhang, W., et al. (2003). A panoramic view of yeast noncoding RNA processing. Cell *113*, 919–933.

Rigaut, G., Shevchenko, A., Rutz, B., Wilm, M., Mann, M., and Seraphin, B. (1999). A generic protein purification method for protein complex characterization and proteome exploration. Nat. Biotechnol. *17*, 1030–1032.

Torchet, C., Bousquet-Antonelli, C., Milligan, L., Thompson, E., Kufel, J., and Tollervey, D. (2002). Processing of 3′-extended read-through transcripts by the exosome can generate functional mRNAs. Mol. Cell *9*, 1285–1296.

van Hoof, A., Lennertz, P., and Parker, R. (2000). Three conserved members of the RNase D family have unique and overlapping functions in the processing of 5S, 5.8S, U4, U5, RNase MRP and RNase P RNAs in yeast. EMBO J. *19*, 1357–1365.

Vanacova, S., Wolf, J., Martin, G., Blank, D., Dettwiler, S., Friedlein, A., Langen, H., Keith, G., and Keller, W. (2005). A new yeast poly(A) polymerase complex involved in RNA quality control. PLoS Biol. *3*, e189. 10.1371/journal.pbio.0030189.

Wyers, F., Rougemaille, M., Badis, G., Rousselle, J.C., Dufour, M.E., Boulay, J., Regnault, B., Devaux, F., Namane, A., Seraphin, B., et al. (2005). Cryptic pol II transcripts are degraded by a nuclear quality control pathway involving a new poly(A) polymerase. Cell *121*, 725–737.

Xie, Z., Johansen, L.K., Gustafson, A.M., Kasschau, K.D., Lellis, A.D., Zilberman, D., Jacobsen, S.E., and Carrington, J.C. (2004). Genetic and functional diversification of small RNA pathways in plants. PLoS Biol. *2*, E104. 10.1371/journal.pbio.0020104.

Xu, J., Yang, J.Y., Niu, Q.W., and Chua, N.H. (2006). Arabidopsis DCP2, DCP1, and VARICOSE form a decapping complex required for postembryonic development. Plant Cell *18*, 3386–3398.

Yamada, K., Lim, J., Dale, J.M., Chen, H., Shinn, P., Palm, C.J., Southwick, A.M., Wu, H.C., Kim, C., Nguyen, M., et al. (2003). Empirical analysis of transcriptional activity in the Arabidopsis genome. Science *302*, 842–846.

Zhang, X., Yazaki, J., Sundaresan, A., Cokus, S., Chan, S.W., Chen, H., Henderson, I.R., Shinn, P., Pellegrini, M., Jacobsen, S.E., and Ecker, J.R. (2006). Genome-wide high-resolution mapping and functional analysis of DNA methylation in arabidopsis. Cell *126*, 1189–1201.

Zilberman, D., Cao, X., Johansen, L.K., Xie, Z., Carrington, J.C., and Jacobsen, S.E. (2004). Role of Arabidopsis ARGONAUTE4 in RNA-directed DNA methylation triggered by inverted repeats. Curr. Biol. *14*, 1214–1220.

Zuo, J., Niu, Q.W., and Chua, N.H. (2000). Technical advance: An estrogen receptor-based transactivator XVE mediates highly inducible gene expression in transgenic plants. Plant J. *24*, 265–273.

Accession Numbers

All raw microarray data (CEL files) for expression analyses were deposited in GEO under the accession number GSE9317. The miRNA168a 3′ end sequences were deposited in GenBank under the accession numbers EU234516–EU234529.